catalysts

MDPI

Article

Influence of Cobalt Precursor on Efficient Production of Commercial Fuels over FTS Co/SiC Catalyst

Ana Raquel de la Osa *, Amaya Romero, Fernando Dorado *, José Luis Valverde and Paula Sánchez

Chemical Engineering Department, Faculty of Chemical Sciences and Technologies, University of Castilla La Mancha, Avda. Camilo José Cela 12, 13071 Ciudad Real, Spain; amaya.romero@uclm.es (A.R.); joseluis.valverde@uclm.es (J.L.V.); paula.sanchez@uclm.es (P.S.)

* Correspondence: anaraquel.osa@uclm.es (A.R.d.l.O.); fernando.dorado@uclm.es (F.D.); Tel.: +34-926-295-300 (ext. 3509) (A.R.d.l.O.); +34-926-295-300 (ext. 3516) (F.D.); Fax: +34-926-295-256 (A.R.d.l.O. & F.D.)

Academic Editor: Michalis Konsolakis

Received: 30 November 2015; Accepted: 28 June 2016; Published: 7 July 2016

Abstract: β-SiC-supported cobalt catalysts have been prepared from nitrate, acetate, chloride and citrate salts to study the dependence of Fischer–Tropsch synthesis (FTS) on the type of precursor. Co*m*/SiC catalysts were synthetized by vacuum-assisted impregnation while N_2 adsorption/desorption, XRD, TEM, TPR, O_2 pulses and acid/base titrations were used as characterization techniques. FTS catalytic performance was carried out at 220 °C and 250 °C while keeping constant the pressure (20 bar), space velocity (6000 $Ncm^3/g{\cdot}h$) and syngas composition (H_2/CO:2). The nature of cobalt precursor was found to influence basic behavior, extent of reduction and metallic particle size. For β-SiC-supported catalysts, the use of cobalt nitrate resulted in big Co crystallites, an enhanced degree of reduction and higher basicity compared to acetate, chloride and citrate-based catalysts. Consequently, cobalt nitrate provided a better activity and selectivity to C_5^+ (less than 10% methane was formed), which was centered in kerosene-diesel fraction ($\alpha = 0.90$). On the contrary, catalyst from cobalt citrate, characterized by the highest viscosity and acidity values, presented a highly dispersed distribution of Co nanoparticles leading to a lower reducibility. Therefore, a lower FTS activity was obtained and chain growth probability was shortened as observed from methane and gasoline-kerosene ($\alpha = 0.76$) production when using cobalt citrate.

Keywords: Fischer–Tropsch; β-SiC support; cobalt precursors; commercial fuels

1. Introduction

In general, there are several factors that affect the performance of Fischer–Tropsch synthesis (FTS) catalysts: media type, nature of the precursor, nature and quantity of promoters as well as dispersion of the active phase [1–3]. Regarding active metal, the production of commercial fuels from syngas is mostly based on supported Co catalysts. Iglesia et al. established that neither the nature of the support nor the dispersion of Co particles influenced turnover frequency (TOF) of these catalysts, but it was proportional to the concentration of active sites on the surface [4–6]. Johnson et al. [7] agree with the fact that TOF was not affected by dispersion, although CO conversion seemed to be strongly dependent on Co reducibility. However, Reuel and Bartholomew [8] or Bessell [9] exposed that both low metal–support interactions and high dispersion are required parameters to obtain a really active cobalt based catalyst. Furthermore, catalysts with high surface density favor the formation of n-paraffins of high molecular weight [4], which is desirable to maximize the production of hydrocarbons in the range of diesel fraction. Hence, at a certain Co loading and established catalyst support, the number of active centers would mainly depend on two parameters, dispersion and degree of reduction of cobalt

oxide supported particles [5,7]. Key in this regard is the strength of the metal–support interaction, which depends largely on the preparation method [10–12] and nature of metal precursor [12–15].

The methods most commonly employed in the preparation of cobalt nitrate based catalysts are vacuum assisted and incipient wetness impregnation (IWI) [5,9]. However, the use of nitrate often results in a catalyst characterized by large Co particles and therefore, a lesser active surface area [16]. On the other hand, a large particle size would favor chain growth probability and low metal–support interactions and therefore, reducibility would be enhanced. For that reason, several authors [13,14,16,17] have studied the influence of the nature of precursor on particle size showing that the use of different salts other than nitrate (acetate, chloride, carbonyl, citrate, EDTA, etc.) results in particles of different size by changing Co^0 dispersion and hence, metal–support interaction. It has been further shown that the final dispersion of metallic cobalt usually depends on the dispersion of Co_3O_4 in the oxidized precursor [18,19].

β-SiC is a ceramic material that despite of a low-to-medium surface area, presents potential properties for its use as support in heterogeneous catalytic processes. These include chemical inertness, excellent mechanical strength and thermal conductivity. In this sense, β-SiC has been tested in several highly endo-/exothermic reactions, including Fischer–Tropsch synthesis [20–26]. Its superior thermal conductivity (one hundred times higher than that of SiO_2 [27]) is of practical interest for FTS since allows hindering hot spots inside the reactor, reducing thermal gradients and consequently, improving plant security and selectivity to heavy hydrocarbons. Nature of precursor of nickel or iron [28] supported over SiC has been investigated showing important differences in catalytic activity. Nonetheless, literature related to the nature of Co/SiC is still scarce and more research is required to improve Co/SiC composition for a highly selective FTS catalyst. Then, the present work was conducted to study the dependence of FTS catalytic performance on the nature of Co metal precursors (nitrate, acetate, chloride and citrate) supported on porous β-SiC.

2. Results and Discussion

Results related to the phase and surface composition, extent of reduction and dispersion of cobalt oxide precursor along with the catalytic activity of Co*m*/β-SiC catalysts are presented and discussed. "*m*" denotes cobalt precursor as N (nitrate), A (acetate), Cl (chloride) and Cit (citrate).

2.1. Thermal Analysis

The decomposition of cobalt precursor is a fundamental stage in the preparation of FTS catalyst since the heat released during this step may affect the structure of cobalt species in the final catalyst and consequently, change reducibility and dispersion [29]. Therefore, in order to determine a proper calcination temperature, thermogravimetric analysis (TG/DTG) of the corresponding parent salts were performed (Figure 1).

Nitrate and cobalt acetate are the most common precursors in the preparation of FTS catalysts. From Figure 1a, it can be observed that in case of the nitrate precursor, there is a progressive weight loss between 25 °C and 210 °C attributable to residual water desorption, while the oxidation of the nitrate ligands occurred at 210–260 °C. The decomposition of cobalt acetate proceeded at slightly higher temperatures, being the main weight loss at 285 °C (Figure 1b). However, from Figure 1c, it can be noted that the decomposition of cobalt chloride took place in several stages, losing water from room temperature to 200 °C and producing dechlorination over 500 °C [30]. Figure 1d shows that cobalt citrate decomposed between 212 °C and 307 °C. It is important to mention that these characterization experiments were run until 600 °C since β-SiC support was reported to be stable under oxidant atmosphere up to this temperature [22,31,32].

Considering the above, and taking into account that supported cobalt catalysts are known to need higher reduction temperatures due to the precursor–support interaction (as demonstrated later by TPR analysis, Section 2.4), higher calcination temperatures are required. In this sense, 550 °C has been recently reported as the optimum calcination temperature for FTS on Co/β-SiC since prevents

deactivation by formation Co_2C species. In addition, the resulting metal–support interaction was found to stabilize cobalt particles against sintering [33]. Therefore, 550 °C was selected as a suitable calcination temperature to completely decompose the precursor into Co_3O_4 as well as to ensure the stability of cobalt species supported on porous β-SiC. In agreement, after calcination step, water appeared to be removed and all ligands were decomposed to the corresponding cobalt oxide phase, as confirmed by XRD measurements (Section 2.3).

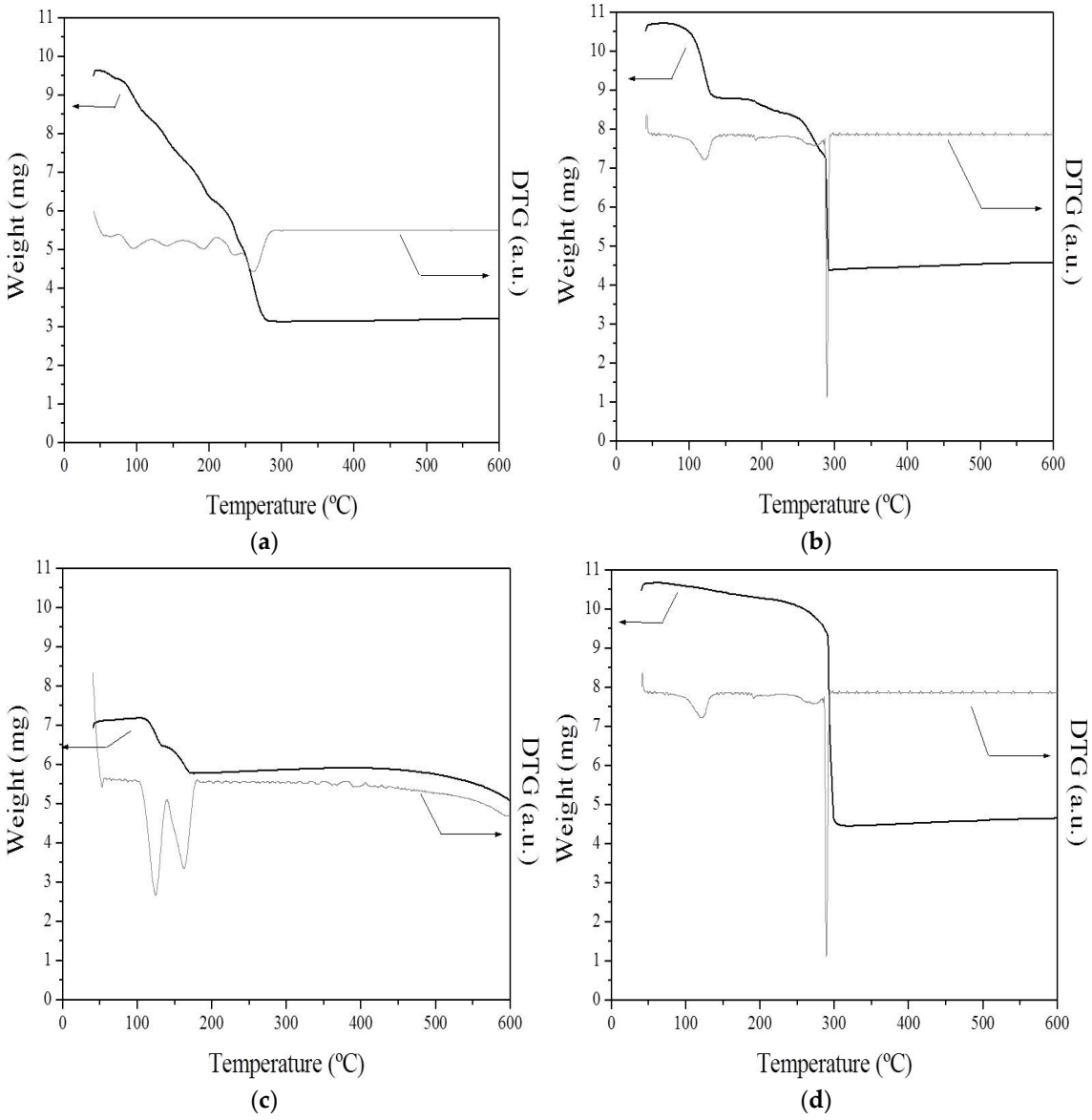

Figure 1. TG/DTG Co precursors: (**a**) CoN; (**b**) CoA; (**c**) CoCl; and (**d**) CoCit.

2.2. Nitrogen Adsorption/Desorption Measurements

Table 1 summarizes textural properties of each oxidized catalyst, estimated from N_2 adsorption–desorption isotherms and BJH method, as described in Section 3.2.3.

Table 1. Physicochemical properties of FTS C*om*/SiC catalysts.

Catalyst	Wt % Co ± 0.1	dCo_3O_4 (nm) [1]	dCo^0 (nm) [11]	D (%) [12]	D (%) [22]	dCo^0 (nm) [2]	Degree of Reduction (%) [3] ± 2	BET Area (m^2/g) [4] ± 1.1	Pore Diameter (nm) [5] ± 0.3	Total Pore Volume (cm^3/g) [6]	Basicity (cm^3/g) [7] ± 0.03
CoN/SiC	9.9	45.0 ± 5.8	33.8	2.8	1.7	56.3 ± 10.1	74.1	21.5	7.2	0.039	0.26
CoCl/SiC	7.2	75.9 ± 8.7	56.9	1.7	2.6	37.1 ± 5.2	41.5	22.1	7.3	0.055	−0.53
CoA/SiC	10.9	34.4 ± 5.2	25.8	3.7	3.6	27.0 ± 5.5	58.5	24.8	8.6	0.106	−1.21
CoCit/SiC	8.9	21.4 ± 4.6	16.1	5.9	5.7	17.0 ± 2.1	41.8	34.9	8.6	0.151	−4.19

[1] Co_3O_4 crystallite size calculated from XRD at 2θ: 36.9°; [11] Co^0 crystallize size from dCo_3O_4 (XRD), Equation (2); [12] Dispersion calculated from XRD Equation (1); [2] Co^0 crystallite size from TEM imaging, Equation (3); [22] Dispersion from TEM imaging Equation (1); [3] Obtained from O_2 Pulses at 400 °C; [4] Calculated by multipoint BET method; [5] Estimated by BJH desorption branch; [6] Determined from a single point of adsorption at $P/P_0 = 0.998$; [7] HCl added (pKi ⩽ 7).

N_2 adsorption/desorption isotherms associated to all of these samples (Figure 2a) show as a combination of isotherms II and IV, as referenced by IUPAC designation. Type II corresponded to the beginning of the isotherm and was caused by adsorption of monolayer/multilayer [34]. Type H3 hysteresis loop observed at higher partial pressures fitted type IV isotherm, characteristic of capillary condensation in presence of mesoporous [35], as denoted by pore distribution (Figure 2b).

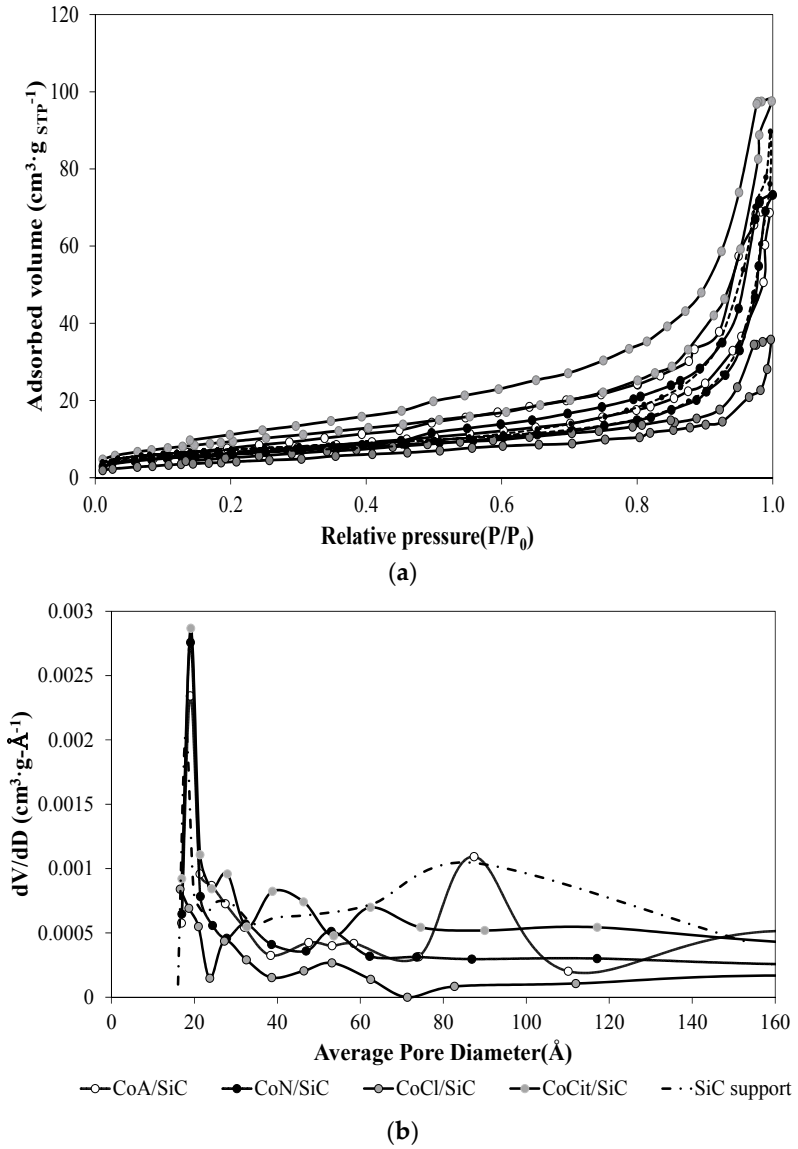

Figure 2. (**a**) N_2 adsorption/desorption isotherms; and (**b**) average pore size distribution.

Moreover, in agreement with isotherms type, pore sizes values shown in Table 1 are within the range of mesopores (2–50 nm) [35]. Particularly, a very similar pore size distribution was found for the four samples, as depicted in Figure 2b, exhibiting a maximum peak ca. 1.9 nm and a second one ca. 8.7 nm, typical of β-SiC support. It should be noted that all samples presented an average Co_3O_4 crystallite size larger than support pore size, as detailed later by means of XRD and TEM imaging, demonstrating that the location of cobalt crystallites on the external surface of β-SiC and not inside its pores may be considered.

From Table 1, it can be also observed that specific surface areas (SA) were similar, 21.5–34.9 m^2/g, within the measurement error range. Upon impregnation of cobalt solutions over β-SiC, a decrease of specific surface area occurred. This effect was significant on CoCl- and CoN-based catalysts,

probably resulting from a partial pore overlay by aggregate particles. However, BET surface area diminished in a lesser extent when cobalt acetate was used as precursor. In addition, pore volume was found to increase probably due to a smaller crystallite size and the slight acid nature of this precursor. It seemed that, for a similar cobalt loading, the more acidic the precursor is, the more amount of metal impurities blocking SiC pores would be eliminated while a lower particle size would be deposited on the support surface, increasing SA and porosity. Accordingly, CoCit/SiC presented the highest total pore volume and SA as detected after acid treatment of silicon carbide catalyst surface [22].

2.3. XRD and TEM

X-ray diffractograms related to β-SiC support, bulk Co_3O_4 and calcined Co*m*/SiC catalysts under study are presented in Figure 3.

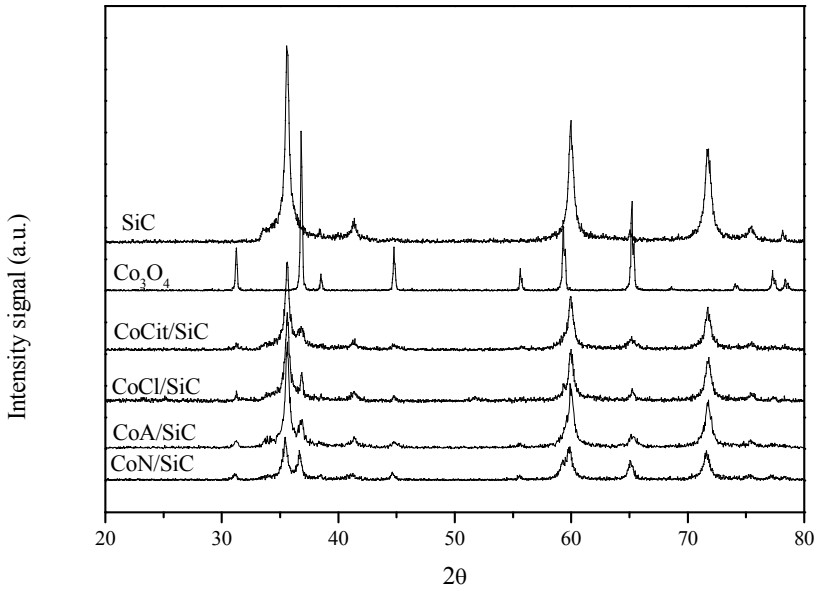

Figure 3. XRD patterns of bulk Co_3O_4, β-SiC support and catalysts Co*m*/SiC.

β-SiC support presented characteristic spectra of the two main SiC polytypes, namely α and β. Reflections at 2θ: 35.5° [111] and 33.7° [0001] are ascribed to hexagonal α-SiC, being the first one (C-SiC) caused by heaping defects generated during the formation of the material [36]. However, those at 2θ: 41.4° [002], 59.9° [202] and 71.7° [113] are assigned to face-centered cubic, β-SiC [37,38]. As depicted in Figure 3, catalyst preparation procedures were confirmed to result in the formation of a pure cobalt oxide spinel phase, Co_3O_4, regardless of the type of precursor. Different to that reported by Cook et al. [39], no evidence of CoO, whose crystal phase arises at 36.5°, 42.4° and 61.5° (JCPDS 75-0393), was found in our samples. Thus, only crystalline Co_3O_4 and β-SiC were detected after calcination.

According to XRD, average Co_3O_4 size related to each synthetized catalyst, deduced from the Scherrer equation at 2θ:36.9°, is listed in Table 1. It was found to increase in the following order: CoCit/SiC < CoA/SiC < CoN/SiC < CoCl/SiC. According to Panpranot et al. [40], cobalt chloride provided the largest particle size and, therefore, the lowest dispersion. It was also noted that, for all samples, particle size was bigger than support pore diameter, which predicts that crystallites of Co oxide were deposited on the outer surface, rather than in the pores of the β-SiC support.

In order to verify the accuracy of XRD characterization results, several TEM micrographs of all the catalysts were collected. Figure 4 shows some examples of TEM images related to Co*m*/SiC catalysts revealing that Co particles disposition on β-SiC support was well determined by the nature of precursor.

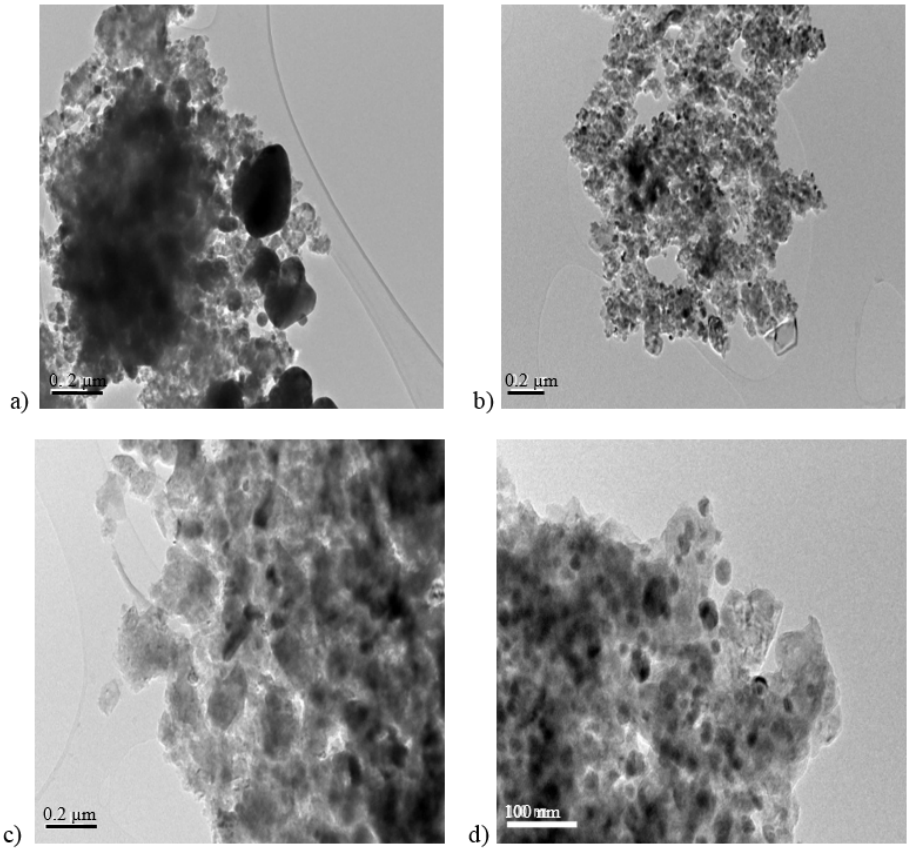

Figure 4. TEM Images: (**a**) CoN/SiC; (**b**) CoA/SiC; (**c**) CoCl/SiC; and (**d**) CoCit/SiC.

TEM image of Figure 4a (CoN/SiC) shows several agglomerates (nm) that turned out to form large Co nanoparticles, even bigger than those expected from XRD. Figure 4b presents a better dispersion of cobalt for CoA/SiC with an average Co^0 particle size of 27 nm, in accordance with XRD data. CoCl/SiC (Figure 5c) displays a broaden size distribution since 15–35 nm crystallites were found to merge into coarse particles. In this case, particle size was proved to be lesser than that of CoN/SiC. In contrast, Figure 4d exhibits a high dispersion of quite fine grains that clumped together in 15–25 nm agglomerates. This also confirms XRD estimation of CoCit/SiC (16–17 nm) crystallite diameter.

Dispersion percentage, D (%), was calculated by assuming spherical cobalt crystallites of uniform diameter (dCo^0) with a site density of 14.6 at/nm^2, using the formula reported by Jones and Bartholomew [41], i.e.,

$$[dp = 96/D] \quad (1)$$

where dp refers to metallic cobalt particle diameter in nm (i.e., dCo^0). Consistent with TEM micrographs in which small crystallites are observed, the oxide produced from decomposition of Co citrate is shown by XRD to be more highly dispersed than the oxides produced from other Co precursors. Considering that both nature of support and average Co^0 size are known to strongly influence cobalt–support interactions, large crystallites of cobalt-nitrate based catalyst were supposed to result in a weaker interaction Co-β-SiC. This fact would lead to a high degree of reduction of cobalt species. It is important to remark that cobalt crystallites on β-SiC support presented globular form, as observed from TEM images, corroborating the proposed hypotheses on spherical particles.

As displayed in Figure 5 average particle size distribution obeyed the series: CoCit/SiC < CoA/SiC < CoCl/SiC < CoN/SiC. The use of citrate as cobalt precursor was confirmed to provide the smallest particle size and a most uniform and narrow disposition (15–20 nm). In case of cobalt acetate and cobalt chloride precursors, particle size distribution was wider, specifically centered on 20 to

30 nm and 30 to 50 nm, verifying estimation from XRD. However, size classification provided by cobalt nitrate was much more heterogeneous, exhibiting a distribution mainly based on medium (35–60 nm) crystallites although the formation of large particles (even higher than 130 nm) from crystalline aggregates was also observed. These data are consistent with XRD diffraction peaks broadening and intensity, indicating heterogeneously distributed large cobalt oxide crystallites, and results reported by Martinez et al. [3] on Co/SBA-15, wherein particle size of cobalt nitrate was bigger than those coming from acetate or acetylacetonate that lead to a higher dispersion and a stronger metal–support interaction. Accordingly, the reducibility of CoN/SiC catalyst should be favored and therefore, its catalytic performance [1,5,42].

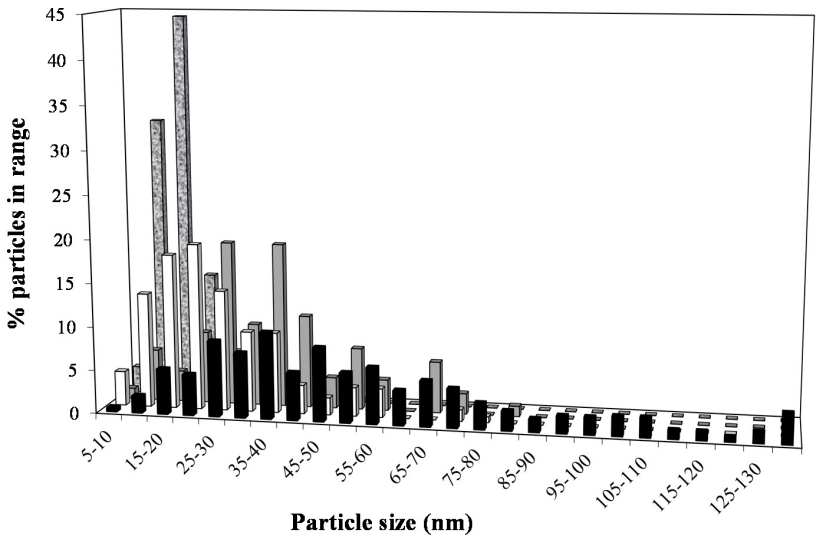

Figure 5. TEM particle size distribution: ■ CoN/SiC; □ CoA/SiC; ▩ CoCl/SiC; and ▨ CoCit/SiC.

As evidenced by XRD and TEM, Co particle size distribution on β-SiC support is attributed to the nature of precursor salts. Cobalt citrate, chloride and acetate proved to be much smaller than that of Co-nitrate based catalyst. Terörde et al. [43] reported that both the viscosity of dissolved salts and their interactions with the support surface are critical parameters in the preparation of iron catalysts by impregnation technique. Thus, citrate precursor was shown to result in a smaller particle size of iron oxide than that of the other precursors used in their study, mainly due to its higher viscosity. Considering this argument, as a result of the drying step, cobalt nitrate crystallizes on β-SiC outer surface, whereas cobalt citrate, which presented a high viscosity, produces a gel that provides well dispersed and scarcely-crystallized species interacting with the support [28].

2.4. Cobalt Oxide Reducibility

Fischer–Tropsch synthesis exclusively proceeds on Co^0 sites. As shown from XRD patterns, Co_3O_4 is the main phase in the prepared catalysts, thus requiring a pretreatment. Despite most of the cobalt is commonly referred to exist as Co^0 phase under reaction conditions, some parameters may hinder reduction step. Co particles would be agglomerated under a high calcination temperature, consequently diminishing the active surface and catalytic performance despite providing a good degree of reduction. On the other hand, small particles frequently lead to a partial degree of reduction [44]. Co particle size and dispersion were found to depend on parent compounds, modifying the corresponding interaction of active sites with the support and therefore, reducibility. Since the degree of reduction of cobalt species seems to play a key role on FTS catalyst activity, the corresponding extent was studied by pulses re-oxidation and TPR techniques.

Figure 6a–e outlines TPR profiles of bulk Co_3O_4 and Co*m*/SiC catalysts, respectively. It is important to mention that a blank test was carried out on fresh β-SiC with no evidence of hydrogen consumption. Hence, TPR peaks can only be attributed to cobalt oxide species reduction.

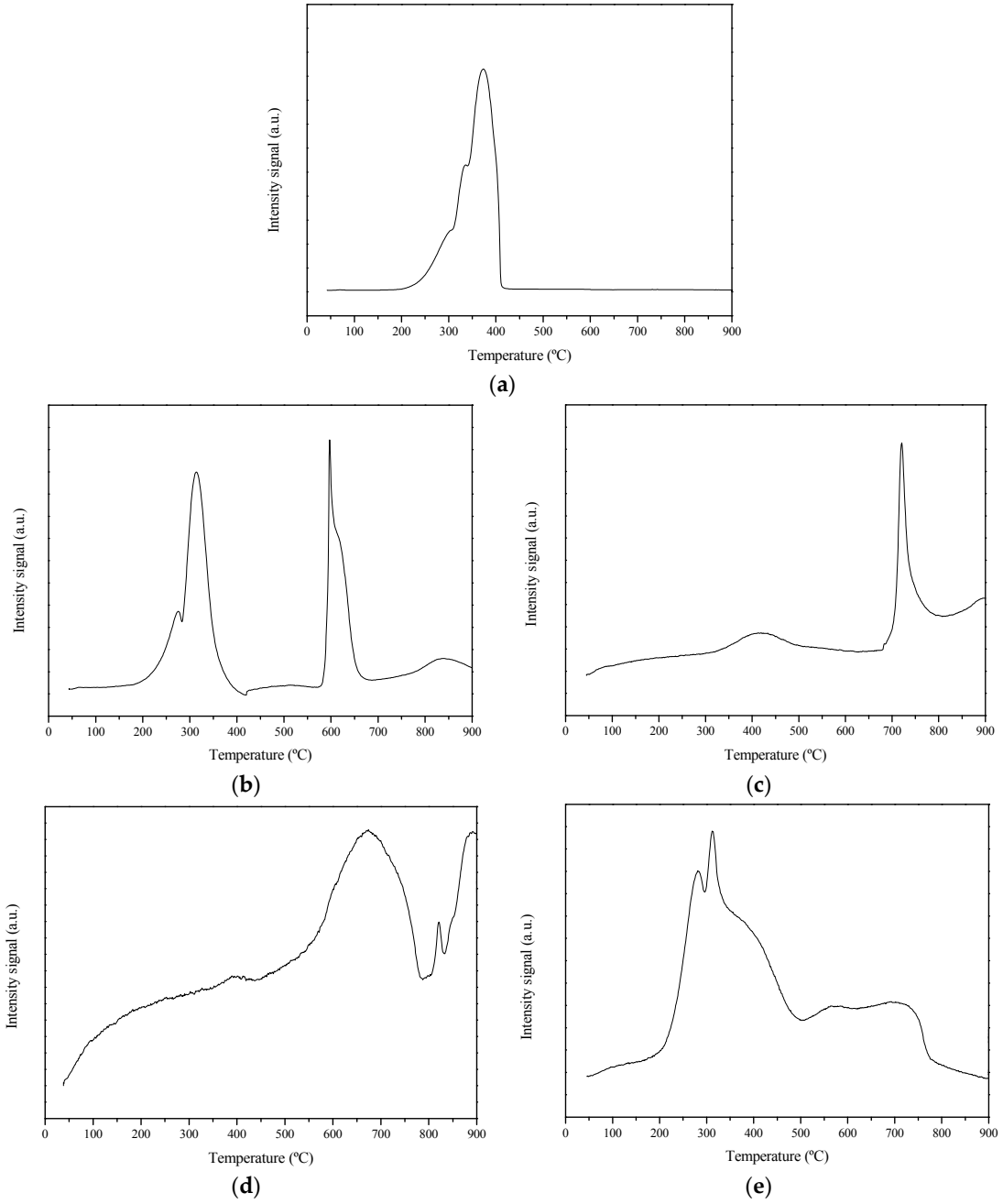

Figure 6. TPR profiles: (**a**) Bulk Co_3O_4; (**b**) CoN/SiC; (**c**) CoA/SiC; (**d**) CoCl/SiC; and (**e**) CoCit/SiC.

It can be seen in Figure 6a that bulk Co_3O_4 was completely reduced to Co^0 at temperatures lower than 350 °C. However, supported cobalt catalysts were expected to show a displacement to higher reduction temperatures. For conventional Co/SiO_2, which is the most similar catalyst to establish a comparison, four TPR reduction peaks are usually reported and identified as: (i) peak α, assigned to Co_3O_4 to CoO reduction; (ii) peak β, related to successive reduction of CoO to Co, at lower temperatures than 400 °C [19]; (iii) peak γ, between 400 °C and 600 °C, referred to mild interaction Co-SiO_2 to Co°; and (iv) peak δ, at temperatures higher than 600 °C, corresponding to Co-silicate/hydrosilicate species to Co^0 [45]. It should be noted that subsequent impregnations could also result in a significant increase in the intensity of high temperature maxima of cobalt silicate structures [46].

In Figure 6b,c, it can be observed that TPR-spectra of catalysts CoN/SiC and CoA/SiC consisted of two main reduction peaks. In agreement with Schanke et al. [19] and Rodrigues et al. [47], and as described above, the first maximum of CoN/SiC at 350 °C could be attributed to the reduction

of Co_3O_4 agglomerates to Co^0 (α and β peaks). The second peak (550–650 °C) was indicative of Co^0 formation from mild-interaction of surface multilayer Co species (CoO_x) [46]. Nevertheless, the presence of immobilized cobalt ions (silicate and hydrosilicates Co-SiO_x species) may not be excluded as revealed by a third small, diffuse maximum between 800 and 850 °C. In the case of catalyst CoA/SiC (Figure 6c), the first maximum of H_2 consumption was observed to be quite lower compared to that of CoN/SiC. Moreover, TPR profile of CoA/SiC was shifted to higher reduction temperatures (420 °C and 720 °C), confirming a lesser degree of reduction due to a stronger interaction between Co species and β-SiC support. This fact would corroborate that catalysts with larger particles are more easily reduced than those with smaller ones, which lead to a higher concentration of hardly reducible cobalt species (silicate-type) [48–50]. TPR profiles associated to CoCl/SiC (Figure 6d) or CoCit/SiC (Figure 6e) resulted to be more complex, showing different Co-species formation upon preparation. Broad maxima indicated the presence of several species reducing at approximately the same temperature, whereas the sharp peaks indicated the existence of a single species. Despite its particle size, a poorer degree of reduction was supposed for catalyst CoCl/SiC compared to CoN/SiC or even CoA/SiC, since its broader profile was found to be widely shifted to higher temperatures. Catalyst CoCit/SiC, presenting the smallest particle size and higher dispersion, also showed a set of overlapped peaks indicating, apart from cobalt oxide reduction (200–450 °C), superposition of mild to strongly immobilized Co species with degrees of different order at temperatures between 500 and 800 °C. Therefore, citrate precursor would provide a diminished degree of reduction to the active phase than that of CoN/SiC.

In order to quantify the reducibility of cobalt oxide precursors, a series of pulse oxidation experiments of reduced samples was developed. The corresponding results, sorted in Table 1, determined that the extent of reduction increased accordingly to: CoCl/SiC~CoCit/SiC < CoA/SiC < CoN/SiC. This trend confirmed that concluded from TPR reduction profiles. It should be mentioned that some authors [51] have found that the degree of reduction may be underestimated for large Co crystallites (10–12 nm) under present pulse oxidation conditions. Titration is then proposed to be conducted at higher O_2 partial pressure (1–2 atm), temperature (450 °C instead of 400 °C), and exposure times (longer than 1 h) to completely oxidize Co^0 to Co_3O_4. In this sense, it should be specified that despite authors have not found evidence of that commented above, large crystallites in this work may subject to the same problem. Therefore, working under suggested conditions may improve the extent of reduction results. In any case, catalyst CoN/SiC would be expected to provide the best FTS catalytic behavior, since it showed a higher extent of reduction. A greater selectivity towards C_5^+ hydrocarbons would be also favored due to its large particle size that would promote chain growth probability [52]. Conversely, theoretically, acid-based (acetate, citrate and especially chloride) samples showed a lower re-oxidation performance, which indicated that a higher amount of Co species were anchored to the support, remarkably decreasing their reducibility.

2.5. Acid-Base Titrations

Finally, since basicity was established to modify C_5^+ hydrocarbon product distribution [52,53], Figure 7 presents the acid-base titration curves of the different catalysts under study.

Titration curves evolved towards higher HCl consumption values as follows: CoCit/SiC < CoA/SiC < CoCl/SiC < CoN/SiC. Table 1 reports surface basicity data, expressed as spent HCl (cm^3) per gram of catalyst sample to reach neutral pH level, confirming differences depending on cobalt precursor. As expected, CoN/SiC was the only catalyst that showed certain basicity with respect to acetate, chloride and citrate, which are postulated as acid ligands. Consequently, in addition to a higher extent of reduction and particle size, as basicity was reported to favor chain growth probability [52,54], this catalyst should result in a shift of C_5^+ hydrocarbon product distribution from gasoline towards higher molecular weights valuable products.

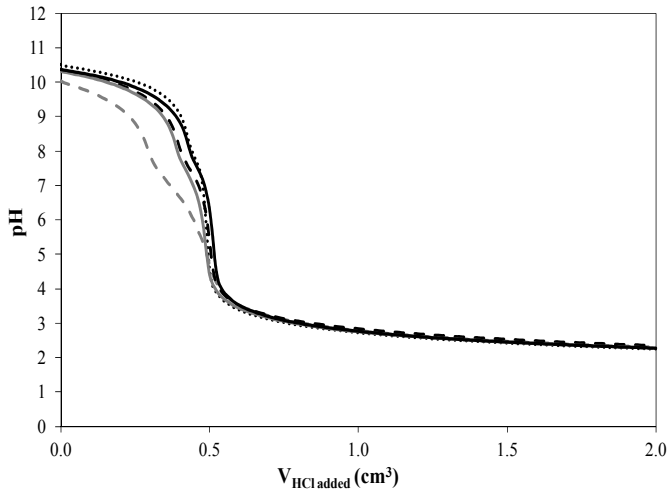

Figure 7. Acid/base titration measurements: ····· Reference; ▬ CoN/SiC; ▬ CoA/SiC; ▬ ▪ CoCl/SiC; and ▬ ▪ CoCit/SiC.

2.6. Fischer–Tropsch Synthesis

In order to study the differences on FTS catalytic performance attributed to the nature of cobalt precursor, a series of catalytic tests were carried out over those synthetized catalysts whose physicochemical characteristics were found to be more diverse, i.e., CoN/SiC and CoCit/SiC. Table 2 collects steady state performance parameters.

Nature of precursor was observed to significantly modify CO conversion and selectivity to C_5^+ hydrocarbons, improving both of them when cobalt nitrate-based catalyst was used. Despite providing a higher CO conversion in the selected range of temperature, CoCit/SiC exhibited a lower catalytic activity when referred to FTS rate. Moreover, this catalyst favored the production of light hydrocarbons (mainly CH_4) and CO_2, compared to CoN/SiC. According to several authors [3,8] and in agreement with characterization results, the increased selectivity to methane can be due to the formation of well dispersed and hardly reducible compounds, which could also catalyze Water Gas Shift reaction, as observed from the increase of CO_2 formation. CoCit/SiC, with a significant acidity, registered a strong Co-β-SiC interaction and deducible low reducibility, then providing low FTS activity. Zhang et al. [55] found that the presence of a relevant amount of acid sites enhanced cobalt–support interactions leading to a lower degree of reduction and a poorer catalytic activity. The chelating ligand facilitated the formation of coordinate species, where Co^{2+} is fixed on the support surface and cobalt-silicate compounds hindered FTS activity. Compared with Co-citrate, CoN/SiC presented Co nanocrystallites whose size, higher than those from the citrate precursor, provided a compromise between an enhanced extent of reduction and a suitable density of active sites, thus improving the performance for FT synthesis. A lower CO conversion was observed at 220 °C for this catalyst, which may occurred due to support pore filling with HC products. It can be seen that, at this temperature, a high selectivity toward C_5^+ hydrocarbons is pointed out and hence, further CO hydrogenation could be prevented by blockage of the active cobalt sites. It is worth it to mention that, under the fixed operating condition, CoN/SiC did not result in CO_2 formation and produced less than 10% of methane, the main FTS side reaction. Moreover, an increase in the reaction temperature was found to only enhance catalytic activity, whereas selectivity to C_5^+ was barely modified when using this catalyst under the fixed range. It should be mentioned that no evidence of catalytic performance deactivation or carbon deposition was found for at least 24 h of reaction, indicating that metal sintering or Boudouard reaction were prevented, probably due to the relatively moderate interaction of Co nanoparticles with β-SiC support, as recently reported by Koo et al. [56].

Regarding FTS selectivity to C_5^+, Table 3 and Figure 8 detailed liquid hydrocarbon product distribution obtained for each catalyst at 250 °C.

Table 2. Influence of cobalt precursor on FTS: 20 bar; 6000 $Ncm^3/g{\cdot}h$; H_2/CO: 1.8.

Catalyst	*T* (°C)	FTS Rate ($mol/mol_{Co}{\cdot}h$) ± 0.4	WGS Rate ($mol/mol_{Co}{\cdot}h$) ± 0.03	Conversion (%) ± 0.5		Selectivity (%)				
				CO	H_2	CO_2 ± 0.03	C_1–C_4 ± 0.4	C_2 OR [1]	C_3 OR [1]	C_5^+ ± 0.4
CoN/SiC	220.00	3.47	0.02	7.40	24.10	0.50	6.20	0.36	1.00	93.30
	235.00	31.50	0.21	67.20	80.20	0.70	5.30	0.09	0.73	94.10
	250.00	34.81	0.41	74.90	85.70	0.70	9.30	0.10	0.72	90.00
CoCit/SiC	220.00	5.69	0.04	24.50	29.80	0.70	9.60	0.09	0.74	89.80
	235.00	17.22	0.74	76.50	89.20	4.10	25.00	0.01	0.19	70.90
	250.00	19.85	1.69	92.30	97.50	7.80	26.50	0.00	0.11	65.70

[1] OR: Olefins ratio calculated as O/O+P where O: Olefins and P: Paraffins; Confidence level 95% (α: 0.05).

Table 3. C_5^+ hydrocarbon distribution: 20 bar; 250 °C; 6000 $Ncm^3/g{\cdot}h$; H_2/CO: 1.8.

Catalyst	C_5^+ Hydrocarbon Distribution (wt %)					Diesel (vol %)	Diesel Yield (%)	α
	Gasoline (C_7–C_{10})	Kerosene (C_{11}–C_{14})	Diesel (C_{15}–C_{18})	Lubricants (C_{19}–C_{20})	Waxes (C_{20}+)			
CoN/SiC	13.3	56.8	23.5	3.2	3.2	17.2	12.9	0.90
CoCit/SiC	56.3	21.1	14.1	4.1	4.8	5.9	5.4	0.76

Confidence level 95% (α: 0.05).

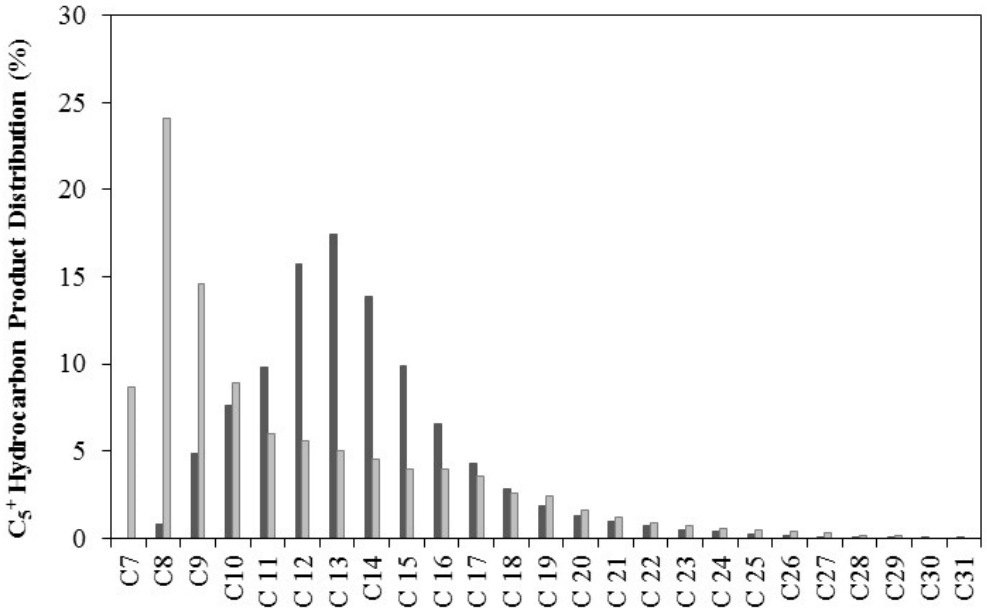

Figure 8. C_5^+ hydrocarbon product distribution: ■ CoCit/SiC; and ■ CoN/SiC. Reaction conditions: 20 bar; 250 °C; 6000 $Ncm^3/g{\cdot}h$; H_2/CO: 2.

FTS selectivity is known to depend on cobalt particle size [1] and basicity [53]. Accordingly, the distribution of C_5^+ hydrocarbons was also modified by the nature of the precursor. Larger cobalt particles are more selective for higher molecular weight hydrocarbons in FTS reaction because of dissociative adsorption of CO, which leads to the formation of -CH_2- required for chain growth. Basicity was also reported to promote chain growth [52,53,57]. It can be observed that catalyst CoCit/SiC, with the smallest particle size and the highest acidity, enhanced the production of gasoline fraction while catalyst CoN/SiC mainly shifted C_5^+ distribution towards the production of kerosene and diesel. It is important to note that although in a lesser extent, the latter reached a diesel yield twice (17%) than that of CoCit/SiC (6%). In agreement, alpha value (α) was set to 0.90 instead of 0.76. Therefore, cobalt nitrate was demonstrated to be the most suitable precursor for the production of synthetic diesel via Fischer–Tropsch synthesis over β-SiC-based catalyst.

3. Experimental Section

3.1. Synthesis of Com/SiC Catalyst

Extrudates of porous β-SiC (1 mm diameter and length, SICAT Catalyst) were used as catalytic support in this study. Medium specific surface area (35 m^2/g) β-SiC was successively vacuum-assisted impregnated with aqueous solutions of: (a) cobalt nitrate (CoN) [$Co(NO_3)_2{\cdot}6H_2O$] (Merck KGaA, Darmstadt, Germany); (b) cobalt chloride (CoCl) [$CoCl_2.6H_2O$] (Panreac Química S.A.U., Barcelona, Spain) or (c) cobalt acetate (CoA) [$C_4H_6CoO_4.4H_2O$] (Panreac Química S.A.U., Barcelona, Spain), in order to prepare a final catalyst with nominal 10 wt % Co loading. β-SiC was precalcined in a SELECTA muffle furnace (224129 model), under static air atmosphere at 550 °C (at a rate of 5 °C/min from ambient temperature) for 6 h before impregnation. Since pore volume of β-silicon carbide support is quite low, synthesis procedure was not based on incipient wetness impregnation technique. In order to obtain the specified Co content, usually, 15 g of β-SiC support were repeatedly impregnated (with intermediate drying) with aqueous solutions comprising the minimum amount of deionized water to dissolve 6.7–8.2 g of cobalt chloride, cobalt acetate or cobalt nitrate. Cobalt concentrations were determined from precursor weight change. After impregnation, the as-prepared mixture was dried in a SELECTA oven (240099 model) under static air atmosphere at 120 °C for 12 h. In addition,

another 10 wt % cobalt-based catalyst was prepared by the citrate method as described elsewhere [58]. Cobalt nitrate was dissolved in an appropriate volume of deionized water to give a 0.1 M solution and then, citric acid [$C_6H_8O_7$] (Panreac Química S.A.U., Barcelona, Spain) was added in 5 wt % excess to guarantee entire complexation. Water was removed at 40 °C, under vacuum, to form a gel that was subsequently dried overnight at 70 °C. The resulting precursor presented a highly hygroscopic nature.

After impregnation and drying steps, all samples were calcined, in the same muffle furnace described above, at 550 °C for 6 h (5 °C/min heating rate) under static air atmosphere, to transform chloride, nitrate, acetate and citrate-ligands into the oxidized phase and then reduced to the Co^0 (Sections 2.4 and 3.3). Each catalyst was denoted as Co*m*/SiC where *m* refers to the cobalt precursor. Physicochemical properties of synthetized Co*m*/SiC are shown in Table 1.

3.2. Catalyst Characterization

3.2.1. Thermal Analysis (TG/DTG)

Thermal analysis over bulk salt precursors (7–12 mg) was conducted in a METTLER TOLEDO model TGA-DSC 1 $STAR_e$ SYSTEM (Mettler-Toledo AG, Schwerzenbach, Switzerland), under oxidant atmosphere. TG/DTG curves were registered from room temperature to 600 °C (5 °C/min heating rate), with an experimental error of ±0.5% in the weight loss measurement and ±2 °C in the temperature measurement.

3.2.2. Atomic Absorption (AA)

The final composition, referred to as wt % Co of calcined catalysts, was determined in a SPECTRAA 220FS (Varian Australia Pty Ltd., Mulgrave, Victoria, Australia), comprising a simple beam and background correction (±1% error). The samples were dissolved in HF before analysis.

3.2.3. Textural Characteristics

A Micromeritics ASAP 2010 sorptometer (Micromeritics, Norcross, GA, USA) was employed to measure porosity and surface area, with an error of ±3%. Catalysts were outgassed under vacuum at 433 K for 16 h before measurement. Total specific surface areas were estimated by the multi-point Brunauer-Emmett-Teller (BET) [59] method using liquid N_2 (77 K) as sorbate, while pore size distributions were determined using Barrett–Joyner–Halenda (BJH) method [60].

3.2.4. X-ray Powder Diffraction

XRD spectra were collected using a Philips model X'Pert MPD (Philips, Eindhoven, the Netherlands) with Co-filtered Cu Kα radiation (λ = 1.54056 Å). Patterns were recorded from 2θ = 3° to 90° with 0.04° step using a 0.4 s acquisition time per step. Crystalline phase's identification after drying and calcination steps was made by comparison to Joint Committee on Powder Diffraction Standards. Co_3O_4 average particle size (dCo_3O_4, nm) was estimated by Scherrer's equation at 2θ:36.9° [61,62]. Then, metallic Co crystallite size (dCo^0, nm) was estimated by Equation (2) [63]:

$$[dCo^0 = 0.75 \cdot dCo_3O_4] \quad (2)$$

3.2.5. Transmission Electron Microscopy

Morphology and structure of the catalysts were characterized by a JEOL 2100 Transmission electron microscope (JEOL USA, Inc.), operated at 200 kV with a resolution of 0.194 nm. The catalysts were reduced ex situ under the same conditions as for FTS testing and then cooled to room temperature and passivated with low oxygen containing mixture (1 vol %) before performing the TEM analysis. Both Co dispersion and diameter distribution were calculated by counting a minimum of 400 particles. Average surface Co particle diameter was evaluated according to Equation (3) [64,65]:

$$[dCo^0 = \sum_i n_i \cdot d_i^3 / \sum_i n_i \cdot d_i^2] \quad (3)$$

where n_i refers to the number of particles with diameter d_i. The standard deviation (σ) of the obtained particle diameter was calculated with the following formula (Equation (4)):

$$[\sigma = \sqrt{\Sigma_i (d_i - \overline{d})^2 / n}] \quad (4)$$

where $\overline{d}$ is the mean Co particle diameter and n the total number of particles.

3.2.6. Temperature Programmed Reduction

Reducibility of Co_3O_4 particles was examined by TPR experiments performed in an Autochem HP 2950 analyzer (Micromeritics, Norcross, GA, USA). Calcined samples were firstly outgassed under flowing argon at 250 °C (10 °C/min heating rate) for 30 min. TPR was then performed using Ar forming gas with 17 *v*/*v* % H_2 as reductant (50 mL/min). Data of temperature and detector signal was monitored from room temperature to 900 °C (5 °C/min heating rate). TPR profiles were consistent, standard deviations for the temperature of the peak maxima being ±2%.

3.2.7. O_2 Pulse

Degree of reduction was calculated in an Autochem HP 2950 (Micromeritics, Norcross, GA, USA) by oxygen titration of reduced samples (±2% average error). After reduction at the same conditions fixed for FTS testing [550 °C (5 °C/min heating rate) for 2 h under pure H_2 (⩾99.9990%) flow], the flow was switched to helium for 1 h to desorb any chemisorbed H_2. Then, O_2 was injected at 400 °C, by means of calibrated pulses in helium carrier, until complete saturation of the catalyst surface (no further O_2 is detected to react with the sample by the TCD) [66]. Calculation of dispersion was based assuming that the H/Co stoichiometric ratio was 1/1 [19], while for the degree of reduction, stoichiometric re-oxidation of Co^0 to Co_3O_4 [67,68] was supposed.

3.2.8. Titrations

A Metrohm 686 apparatus (Metrohm Ltd., Herisau, Switzerland) was used to conduct acid/base titrations. 25 mg of catalyst were dissolved in 50 cm^3 of a NaCl solution (0.1 M, also used as a reference) and basified to pH = 10.3 (0.1 M NaOH). Then, titrant (0.1 M HCl) was dosed by an automatic Dosimat 665 at a rate of 3 cm^3/h under constant stirring and N_2 atmosphere.

3.3. Activity Test

FTS experiments were conducted in a bench scale, fully automated facility, under a pressure of 20 bar, as described elsewhere [24]. Typically, 5 g of catalyst dispersed on inert α-SiC (in a 1:4 wt. ratio in order to minimize temperature gradients) were charged into the reactor (1 m length and 1.77 cm internal diameter, comprising a volume of 0.24 L, made of Inconel 600). The catalyst was firstly pretreated by reduction in pure H_2 (⩾99.999%) flow (1.5 NL/min) at 550 °C (5 °C/min heating rate) under atmospheric pressure for 2 h. Then, temperature was decreased to the required reaction temperature under flowing N_2 while pressure was set on 20 bars. FTS catalytic performance was then studied at 220 °C, 235 °C and 250 °C, a gas space velocity of 6000 $Ncm^3/g{\cdot}h$ and a molar ratio H_2/CO of 1.8 (considering a previous Water Gas Shift stage). Temperature was checked (with an error of ±0.5 °C) in the bed of catalyst and along the whole tube through a series of thermocouples disposed to control temperature gradients in the fixed-bed reactor. The feed gas consisted of highly pure N_2 (10 vol %), CO (60 vol %), and H_2 (30 vol %), being N_2 the internal standard used to ensure an accurate carbon balance. Downstream, a Peltier cell was located prior to the analysis system in order to separate non-condensate water and to avoid overpressure on the input of the chromatographic unit. Light hydrocarbons and unreacted reactants were analyzed online every 90 min, using a CP-4900 Varian microgas chromatograph equipped with: (a) a Molsieve 5A capillary column (H_2, N_2, CH_4 and CO); and (b) a Pora Pack Q capillary column (CO_2, ethane and propane). C_5^+ hydrocarbons, collected for 8–12 h to ensure reaching the steady state, were extracted with n-hexane from liquid products

stream. After this step, organic phase was analyzed offline in a gas chromatograph equipped with a FID detector and an ultrafast capillary column, supplied by Thermo Fisher Scientific. Hydrocarbon selectivity was estimated as reported elsewhere [23]. Three replicate experiments were randomized conducted in order to avoid systematic errors while quantifying reproducibility of each precursor system. Confidence interval was calculated from experimental data by means of the Student test (*t*-test, 95% confidence level), and the corresponding standard deviation measurement.

4. Conclusions

This work explored the dependence of FTS catalytic performance on cobalt precursor supported on β-SiC. The use of different parent cobalt compounds significantly modified physicochemical characteristics of Co*m*/SiC catalyst and, therefore, their FTS catalytic performance. There was an increase in the basicity of the catalyst in the following order: CoCit/SiC < CoA/SiC < CoCl/SiC < CoN/SiC. The same trend was found for the average Co particle size, although a wide distribution was found for CoCl/SiC and CoN/SiC, affecting the extent of reduction. Consequently, FTS activity and chain growth probability were found to depend on the nature of the precursor used for the preparation of Co*m*/SiC catalysts. The use of an organic compound such as cobalt citrate resulted in a significant increase of dispersion, exhibiting a homogeneous disposition of small cobalt crystallites on β-SiC compared with those from CoN/SiC. Consequently, citrate-based catalyst provided a lower FTS rate and an enhanced selectivity to CO_2 and C_1–C_4 fraction. Moreover, cobalt citrate also led to a C_5^+ product distribution centered on gasoline fraction ($\alpha = 0.76$). Nevertheless, cobalt nitrate, related to the highest particle size, degree of reduction and basicity, resulted in a better FTS activity with a low formation of CH_4, shifting the production of C_5^+ hydrocarbons towards kerosene-diesel fraction (0.90), with diesel yield twice that produced by CoCit/SiC.

Acknowledgments: Financial supports were provided by the Ministerio de Industria, Turismo y Comercio of Spain (CENIT-PiIBE project) and ELCOGAS S.A. Sicat catalyst is also gratefully acknowledged for providing support sample.

Author Contributions: A.R. de la Osa prepared the catalysts, performed the experiments and wrote the original manuscript. P. Sánchez helped to prepare the final manuscript and revised the final version of the paper. F. Dorado, A. Romero and J.L. Valverde revised the final version of the paper.

Conflicts of Interest: The authors declare no conflict of interest.

References

1. Borg, Ø.; Eri, S.; Blekkan, E.A.; Storsæter, S.; Wigum, H.; Rytter, E.; Holmen, A. Fischer-Tropsch synthesis over γ-alumina-supported cobalt catalysts: Effect of support variables. *J. Catal.* **2007**, *248*, 89–100. [CrossRef]
2. Jacobs, G.; Ji, Y.; Davis, B.H.; Cronauer, D.; Kropf, A.J.; Marshall, C.L. Fischer-Tropsch synthesis: Temperature programmed EXAFS/XANES investigation of the influence of support type, cobalt loading, and noble metal promoter addition to the reduction behavior of cobalt oxide particles. *Appl. Catal. A* **2007**, *333*, 177–191. [CrossRef]
3. Martínez, A.N.; López, C.; Márquez, F.; Díaz, I. Fischer-Tropsch synthesis of hydrocarbons over mesoporous Co/SBA-15 catalysts: The influence of metal loading, cobalt precursor, and promoters. *J. Catal.* **2003**, *220*, 486–499. [CrossRef]
4. Iglesia, E. Design, synthesis, and use of cobalt-based Fischer-Tropsch synthesis catalysts. *Appl. Catal. A* **1997**, *161*, 59–78. [CrossRef]
5. Iglesia, E.; Soled, S.L.; Fiato, R.A. Fischer-Tropsch synthesis on cobalt and ruthenium. Metal dispersion and support effects on reaction rate and selectivity. *J. Catal.* **1992**, *137*, 212–224. [CrossRef]
6. Iglesia, E.; Reyes, S.C.; Madon, R.J.; Soled, S.L. Selectivity control and catalyst design in the Fischer-Tropsch synthesis: Sites, pellets, and reactors. *Adv. Catal.* **1993**, *39*, 221–302.
7. Johnson, B.G.; Bartholomew, C.H.; Goodman, D.W. The role of surface structure and dispersion in CO hydrogenation on cobalt. *J. Catal.* **1991**, *128*, 231–247. [CrossRef]
8. Reuel, R.C.; Bartholomew, C.H. Effects of support and dispersion on the CO hydrogenation activity/selectivity properties of cobalt. *J. Catal.* **1984**, *85*, 78–88. [CrossRef]

9. Bessell, S. Support effects in cobalt-based Fischer-Tropsch catalysis. *Appl. Catal. A* **1993**, *96*, 253–268. [CrossRef]
10. Clause, O.; Kermarec, M.; Bonneviot, L.; Villain, F.; Che, M. Nickel(II) ion-support interactions as a function of preparation method of silica-supported nickel materials. *J. Am. Chem. Soc.* **1992**, *114*, 4709–4717. [CrossRef]
11. Lekhal, A.; Glasser, B.J.; Khinast, J.G. Influence of pH and ionic strength on the metal profile of impregnation catalysts. *Chem. Eng. Sci.* **2004**, *59*, 1063–1077. [CrossRef]
12. Van de Water, L.G.A.; Bezemer, G.L.; Bergwerff, J.A.; Versluijs-Helder, M.; Weckhuysen, B.M.; de Jong, K.P. Spatially resolved UV-VIS microspectroscopy on the preparation of alumina-supported Co Fischer-Tropsch catalysts: Linking activity to Co distribution and speciation. *J. Catal.* **2006**, *242*, 287–298. [CrossRef]
13. Rosynek, M.P.; Polansky, C.A. Effect of cobalt source on the reduction properties of silica-supported cobalt catalysts. *Appl. Catal.* **1991**, *73*, 97–112. [CrossRef]
14. Niemelä, M.K.; Krause, A.O.I.; Vaara, T.; Lahtinen, J. Preparation and characterization of Co/SiO_2, $Co\text{-}Mg/SiO_2$ and $Mg\text{-}Co/SiO_2$ catalysts and their activity in CO hydrogenation. *Top. Catal.* **1995**, *2*, 45–57. [CrossRef]
15. Niemelä, M.K.; Krause, A.O.I. The long-term performance of Co/SiO_2 catalysts in CO hydrogenation. *Catal. Lett.* **1996**, *42*, 161–166. [CrossRef]
16. Van de Loosdrecht, J.; Van der Haar, M.; Van der Kraan, A.M.; Van Dillen, A.J.; Geus, J.W. Preparation and properties of supported cobalt catalysts for Fischer-Tropsch synthesis. *Appl. Catal. A Gen.* **1997**, *150*, 365–376. [CrossRef]
17. Matsuzaki, T.; Takeuchi, K.; Hanaoka, T.; Arakawa, H.; Sugi, Y. Hydrogenation of carbon monoxide over highly dispersed cobalt catalysts derived from cobalt(II) acetate. *Catal. Today* **1996**, *28*, 251–259. [CrossRef]
18. Sun, S.; Tsubaki, N.; Fujimoto, K. The reaction performances and characterization of Fischer-Tropsch synthesis Co/SiO_2 catalysts prepared from mixed cobalt salts. *Appl. Catal. A* **2000**, *202*, 121–131. [CrossRef]
19. Schanke, D.; Vada, S.; Blekkan, E.A.; Hilmen, A.M.; Hoff, A.; Holmen, A. Study of Pt-promoted cobalt CO hydrogenation catalysts. *J. Catal.* **1995**, *156*, 85–95. [CrossRef]
20. Lacroix, M.; Dreibine, L.; De Tymowski, B.; Vigneron, F.; Edouard, D.; Bégin, D.; Nguyen, P.; Pham, C.; Savin-Poncet, S.; Luck, F.; et al. Silicon carbide foam composite containing cobalt as a highly selective and re-usable Fischer-Tropsch synthesis catalyst. *Appl. Catal. A* **2011**, *397*, 62–72. [CrossRef]
21. De Tymowski, B.; Liu, Y.; Meny, C.; Lefèvre, C.; Begin, D.; Nguyen, P.; Pham, C.; Edouard, D.; Luck, F.; Pham-Huu, C. Co-Ru/SiC impregnated with ethanol as an effective catalyst for the Fischer-Tropsch synthesis. *Appl. Catal. A* **2012**, *419–420*, 31–40. [CrossRef]
22. Díaz, J.A.; Calvo-Serrano, M.; De la Osa, A.R.; García-Minguillán, A.M.; Romero, A.; Giroir-Fendler, A.; Valverde, J.L. β-silicon carbide as a catalyst support in the Fischer-Tropsch synthesis: Influence of the modification of the support by a pore agent and acidic treatment. *Appl. Catal. A* **2014**, *475*, 82–89. [CrossRef]
23. De la Osa, A.R.; De Lucas, A.; Díaz-Maroto, J.; Romero, A.; Valverde, J.L.; Sánchez, P. FTS fuels production over different Co/SiC catalysts. *Catal. Today* **2012**, *187*, 173–182. [CrossRef]
24. De la Osa, A.R.; De Lucas, A.; Sánchez-Silva, L.; Díaz-Maroto, J.; Valverde, J.L.; Sánchez, P. Performing the best composition of supported Co/SiC catalyst for selective FTS diesel production. *Fuel* **2012**, *95*, 587–598. [CrossRef]
25. Lee, B.; Koo, H.; Park, M.-J.; Lim, B.; Moon, D.; Yoon, K.; Bae, J. Deactivation behavior of Co/SiC Fischer-Tropsch catalysts by formation of filamentous carbon. *Catal. Lett.* **2013**, *143*, 18–22. [CrossRef]
26. Lee, J.S.; Jung, J.S.; Moon, D.J. The effect of cobalt loading on Fischer-Tropsch synthesis over silicon carbide supported catalyst. *J. Nanosci. Nanotechnol.* **2015**, *15*, 396–399. [CrossRef] [PubMed]
27. Zhu, X.; Lu, X.; Liu, X.; Hildebrandt, D.; Glasser, D. Heat transfer study with and without Fischer-Tropsch reaction in a fixed bed reactor with TiO_2, SiO_2, and SiC supported cobalt catalysts. *Chem. Eng. J.* **2014**, *247*, 75–84. [CrossRef]
28. Torres Galvis, H.M.; Koeken, A.C.J.; Bitter, J.H.; Davidian, T.; Ruitenbeek, M.; Dugulan, A.I.; De Jong, K.P. Effect of precursor on the catalytic performance of supported iron catalysts for the Fischer-Tropsch synthesis of lower olefins. *Catal. Today* **2013**, *215*, 95–102. [CrossRef]
29. Khodakov, A.Y. Enhancing cobalt dispersion in supported Fischer-Tropsch catalysts via controlled decomposition of cobalt precursors. *Braz. J. Phys.* **2009**, *39*, 171–175. [CrossRef]
30. Mishra, S.K.; Kanungo, S.B. Thermal dehydration and decomposition of cobalt chloride hydrate ($CoCl_2 \cdot xH_2O$). *J. Therm. Anal.* **1992**, *38*, 2437–2454. [CrossRef]

31. Yuan, X.; Lü, J.; Yan, X.; Hu, L.; Xue, Q. Preparation of ordered mesoporous silicon carbide monoliths via preceramic polymer nanocasting. *Microporous Mesoporous Mater.* **2011**, *142*, 754–758. [CrossRef]
32. Jacobson, N.S.; Myers, D.L. Active oxidation of SiC. *Oxid. Met.* **2011**, *75*, 1–25. [CrossRef]
33. Labuschagne, J.; Meyer, R.; Chonco, Z.H.; Botha, J.M.; Moodley, D.J. Application of water-tolerant Co/β-SiC catalysts in slurry phase Fischer-Tropsch synthesis. *Catal. Today* **2016**. [CrossRef]
34. Kolasinski, K.W. *Surface Science Foundations of Catalysis and Nanoscience*; John Wiley and Sons: Chichester, UK, 2007.
35. Sing, K.S.W.; Everett, D.H.; Haul, R.A.W.; Moscou, L.; Pierotti, R.A.; Rouquerol, J.; Siemieniewska, T. Reporting Physisorption Data for Gas/Solid Systems with Special Reference to the Determination of Surface Area and Porosity. *Pure Appl. Chem.* **1985**, *57*, 603–619. [CrossRef]
36. Nguyen, P.; Pham, C. Innovative porous SiC-based materials: From nanoscopic understandings to tunable carriers serving catalytic needs. *Appl. Catal. A* **2011**, *391*, 443–454. [CrossRef]
37. Ledoux, M.J.; Pham-Huu, C. Silicon carbide a novel catalyst support for heterogeneous catalysis. *Cattech* **2001**, *5*, 226–246. [CrossRef]
38. Lee, S.-H.; Yun, S.-M.; Kim, S.; Park, S.-J.; Lee, Y.-S. Characterization of nanoporous β-SiC fiber complex prepared by electrospinning and carbothermal reduction. *Res. Chem. Intermed.* **2010**, *36*, 731–742. [CrossRef]
39. Cook, K.M.; Poudyal, S.; Miller, J.T.; Bartholomew, C.H.; Hecker, W.C. Reducibility of alumina-supported cobalt Fischer-Tropsch catalysts: Effects of noble metal type, distribution, retention, chemical state, bonding, and influence on cobalt crystallite size. *Appl. Catal. A* **2012**, *449*, 69–80. [CrossRef]
40. Panpranot, J.; Kaewkun, S.; Praserthdam, P.; Goodwin, J., Jr. Effect of cobalt precursors on the dispersion of cobalt on MCM-41. *Catal. Lett.* **2003**, *91*, 95–102. [CrossRef]
41. Jones, R.D.; Bartholomew, C.H. Improved flow technique for measurement of hydrogen chemisorption on metal catalysts. *Appl. Catal.* **1988**, *39*, 77–88. [CrossRef]
42. Belambe, A.R.; Oukaci, R.; Goodwin, J.G., Jr. Effect of pretreatment on the activity of a Ru-promoted Co/Al_2O_3 Fischer-Tropsch catalyst. *J. Catal.* **1997**, *166*, 8–15. [CrossRef]
43. Terörde, R.J.A.M.; Van den Brink, P.J.; Visser, L.M.; Van Dillen, A.J.; Geus, J.W. Selective oxidation of hydrogen sulfide to elemental sulfur using iron oxide catalysts on various supports. *Catal. Today* **1993**, *17*, 217–224. [CrossRef]
44. Sun, S.; Fujimoto, K.; Yoneyama, Y.; Tsubaki, N. Fischer-Tropsch synthesis using Co/SiO_2 catalysts prepared from mixed precursors and addition effect of noble metals. *Fuel* **2002**, *81*, 1583–1591. [CrossRef]
45. Zhou, W.; Chen, J.-G.; Fang, K.-G.; Sun, Y.-H. The deactivation of Co/SiO_2 catalyst for Fischer-Tropsch synthesis at different ratios of H_2 to CO. *Fuel Process. Technol.* **2006**, *87*, 609–616. [CrossRef]
46. Solomonik, I.G.; Gryaznov, K.O.; Skok, V.F.; Mordkovich, V.Z. Formation of surface cobalt structures in SiC-supported Fischer-Tropsch catalysts. *RSC Adv.* **2015**, *5*, 78586–78597. [CrossRef]
47. Rodrigues, E.L.; Bueno, J.M.C. Co/SiO_2 catalysts for selective hydrogenation of crotonaldehyde II: Influence of the Co surface structure on selectivity. *Appl. Catal. A* **2002**, *232*, 147–158. [CrossRef]
48. Bechara, R.; Balloy, D.; Dauphin, J.-Y.; Grimblot, J. Influence of the characteristics of γ-aluminas on the dispersion and the reducibility of supported cobalt catalysts. *Chem. Mater.* **1999**, *11*, 1703–1711. [CrossRef]
49. Ernst, B.; Bensaddik, A.; Hilaire, L.; Chaumette, P.; Kiennemann, A. Study on a cobalt silica catalyst during reduction and Fischer-Tropsch reaction: In situ EXAFS compared to XPS and XRD. *Catal. Today* **1998**, *39*, 329–341. [CrossRef]
50. Khodakov, A.Y.; Lynch, J.; Bazin, D.; Rebours, B.; Zanier, N.; Moisson, B.; Chaumette, P. Reducibility of cobalt species in silica-supported Fischer-Tropsch catalysts. *J. Catal.* **1997**, *168*, 16–25. [CrossRef]
51. Keyvanloo, K.; Fisher, M.J.; Hecker, W.C.; Lancee, R.J.; Jacobs, G.; Bartholomew, C.H. Kinetics of deactivation by carbon of a cobalt Fischer-Tropsch catalyst: Effects of CO and H_2 partial pressures. *J. Catal.* **2015**, *327*, 33–47. [CrossRef]
52. Bao, A.; Liew, K.; Li, J. Fischer-Tropsch synthesis on CaO-promoted Co/Al_2O_3 catalysts. *J. Mole. Cataly. A* **2009**, *304*, 47–51. [CrossRef]
53. De la Osa, A.R.; De Lucas, A.; Valverde, J.L.; Romero, A.; Monteagudo, I.; Coca, P.; Sánchez, P. Influence of alkali promoters on synthetic diesel production over Co catalyst. *Catal. Today* **2011**, *167*, 96–106. [CrossRef]
54. Dry, M.E.; Oosthuizen, G.J. The correlation between catalyst surface basicity and hydrocarbon selectivity in the Fischer-Tropsch synthesis. *J. Catal.* **1968**, *11*, 18–24. [CrossRef]

55. Zhang, J.; Chen, J.; Ren, J.; Sun, Y. Chemical treatment of γ-Al_2O_3 and its influence on the properties of Co-based catalysts for Fischer-Tropsch synthesis. *Appl. Catal. A* **2003**, *243*, 121–133. [CrossRef]
56. Koo, H.-M.; Lee, B.S.; Park, M.-J.; Moon, D.J.; Roh, H.-S.; Bae, J.W. Fischer-Tropsch synthesis on Cobalt/Al_2O_3-modified SiC catalysts: Effect of cobalt-alumina interactions. *Catal. Sci. Technol.* **2014**, *4*, 343–351. [CrossRef]
57. Zhang, J.; Chen, J.; Ren, J.; Li, Y.; Sun, Y. Support effect of Co/Al_2O_3 catalysts for Fischer-Tropsch synthesis. *Fuel* **2003**, *82*, 581–586. [CrossRef]
58. Courty, P.; Ajot, H.; Marcilly, C.; Delmon, B. Oxydes mixtes ou en solution solide sous forme très divisée obtenus par décomposition thermique de précurseurs amorphes. *Powder Technol.* **1973**, *7*, 21–38. [CrossRef]
59. Brunauer, S.; Emmett, P.H.; Teller, E. Adsorption of gases in multimolecular layers. *J. Am. Chem. Soc.* **1938**, *60*, 309–319. [CrossRef]
60. Barrett, E.P.; Joyner, L.G.; Halenda, P.P. The determination of pore volume and area distributions in porous substances. I. Computations from nitrogen isotherms. *J. Am. Chem. Soc.* **1951**, *73*, 373–380. [CrossRef]
61. Scherrer, P. Bestimmung der Größe und der inneren Struktur von Kolloidteilchen mittels Röntgenstrahlen. Nachrichten von der Gesellschaft der Wissenschaften zu Göttingen. *Mathematisch-Physikalische Klasse* **1918**, *2*, 98–100.
62. Klug, H.P.; Alexander, L.E. *X-ray Diffraction Procedures for Polycrystalline Amorphous Materials*, 2nd ed.; Wiley: New York, NY, USA, 1974; p. 992.
63. Van 't Blik, H.F.J.; Koningsberger, D.C.; Prins, R. Characterization of supported cobalt and Cobalt-Rhodium catalysts. III. Temperature-programmed reduction (TPR), oxidation (TPO), and EXAFS of CoRh SiO_2. *J. Catal.* **1986**, *97*, 210–218. [CrossRef]
64. Datye, A.K.; Xu, Q.; Kharas, K.C.; McCarty, J.M. Particle size distributions in heterogeneous catalysts: What do they tell us about the sintering mechanism? *Catal. Today* **2006**, *111*, 59–67. [CrossRef]
65. Mustard, D.G.; Bartholomew, C.H. Determination of metal crystallite size and morphology in supported nickel catalysts. *J. Catal.* **1981**, *67*, 186–206. [CrossRef]
66. Bartholomew, C.H.; Farrauto, R.J. Chemistry of nickel-alumina catalysts. *J. Catal.* **1976**, *45*, 41–53. [CrossRef]
67. Song, D.; Li, J. Effect of catalyst pore size on the catalytic performance of silica supported cobalt Fischer-Tropsch catalysts. *J. Mol. Catal. A* **2006**, *247*, 206–212. [CrossRef]
68. Jacobs, G.; Das, T.K.; Zhang, Y.; Li, J.; Racoillet, G.; Davis, B.H. Fischer-Tropsch synthesis: Support, loading, and promoter effects on the reducibility of cobalt catalysts. *Appl. Catal. A* **2002**, *233*, 263–281. [CrossRef]